LETTER

doi:10.1038/nature12957

Drought sensitivity of Amazonian carbon balance revealed by atmospheric measurements

L. V. Gatti[1]*, M. Gloor[2]*, J. B. Miller[3,4]*, C. E. Doughty[5], Y. Malhi[5], L. G. Domingues[1], L. S. Basso[1], A. Martinewski[1], C. S. C. Correia[1], V. F. Borges[1], S. Freitas[6], R. Braz[6], L. O. Anderson[5,7], H. Rocha[8], J. Grace[9], O. L. Phillips[2] & J. Lloyd[10,11]

Feedbacks between land carbon pools and climate provide one of the largest sources of uncertainty in our predictions of global climate[1,2]. Estimates of the sensitivity of the terrestrial carbon budget to climate anomalies in the tropics and the identification of the mechanisms responsible for feedback effects remain uncertain[3,4]. The Amazon basin stores a vast amount of carbon[5], and has experienced increasingly higher temperatures and more frequent floods and droughts over the past two decades[6]. Here we report seasonal and annual carbon balances across the Amazon basin, based on carbon dioxide and carbon monoxide measurements for the anomalously dry and wet years 2010 and 2011, respectively. We find that the Amazon basin lost 0.48 ± 0.18 petagrams of carbon per year (Pg C yr^{-1}) during the dry year but was carbon neutral (0.06 ± 0.1 Pg C yr^{-1}) during the wet year. Taking into account carbon losses from fire by using carbon monoxide measurements, we derived the basin net biome exchange (that is, the carbon flux between the non-burned forest and the atmosphere) revealing that during the dry year, vegetation was carbon neutral. During the wet year, vegetation was a net carbon sink of 0.25 ± 0.14 Pg C yr^{-1}, which is roughly consistent with the mean long-term intact-forest biomass sink of 0.39 ± 0.10 Pg C yr^{-1} previously estimated from forest censuses[7]. Observations from Amazonian forest plots suggest the suppression of photosynthesis during drought as the primary cause for the 2010 sink neutralization. Overall, our results suggest that moisture has an important role in determining the Amazonian carbon balance. If the recent trend of increasing precipitation extremes persists[6], the Amazon may become an increasing carbon source as a result of both emissions from fires and the suppression of net biome exchange by drought.

To observe the state, changes and climate sensitivity of the Amazon carbon pools we initiated a lower-troposphere greenhouse-gas sampling programme over the Amazon basin in 2010, measuring bi-weekly vertical profiles of carbon dioxide (CO_2), sulphur hexafluoride (SF_6) and carbon monoxide (CO) from just above the forest canopy to 4.4 km above sea level (a.s.l.) at four locations spread across the basin (Fig. 1). Repeated measurements of the CO_2 mole fraction in the low to mid-troposphere have the ability to constrain surface CO_2 fluxes at regional scales (about 10^5–10^6 km^2) including all known and unknown processes. This is in contrast to small temporal[8,9] and spatial[10,11] scale atmospheric approaches, which need substantial and difficult-to-verify assumptions to scale up; it is also in contrast to basin-scale surface-based studies, which include only a subset of relevant processes[3,12,13].

Our selection of sites reflects the dominant mode of horizontal air flow at mid- to low-troposphere altitudes across the Amazon basin, with air entering the basin from the equatorial Atlantic Ocean, sweeping over the tropical forested region towards the Andes and turning southwards and back to the Atlantic (Fig. 1). Air at the end-of-the-basin sites Tabatinga (TAB) and Rio Branco (RBA) is thus exposed to carbon fluxes from a large fraction of the basin's rainforest vegetation. Flux signatures

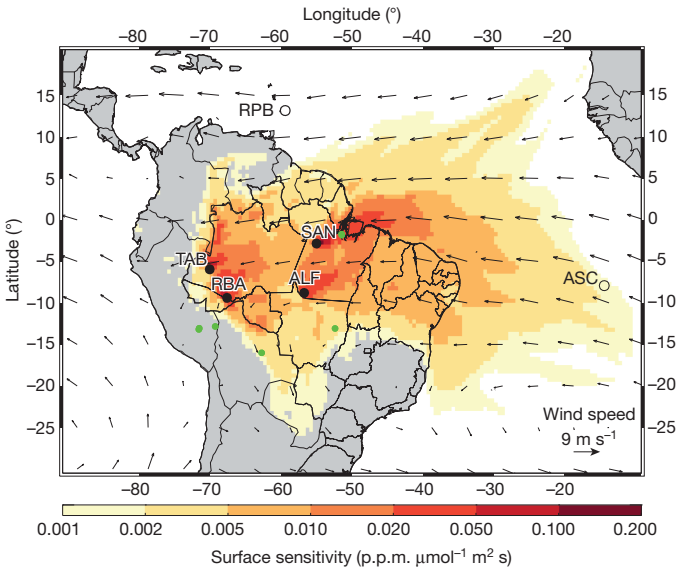

Figure 1 | Station's region of influence ('footprint'). The combined sensitivity of all observed atmospheric CO_2 concentrations to surface fluxes (that is, measurement 'footprints') is shown for the four sites TAB, RBA, SAN and ALF (solid black dots). Sensitivity is given in units of concentration (p.p.m.) per unit flux (μmol m^{-2} s^{-1}). As seen in Extended Data Fig. 6a, footprints from the four sites overlap substantially. Footprints are calculated at 0.5-degree resolution using ensembles of stochastically generated back trajectories using the FLEXPART Lagrangian particle dispersion model and then calculating the residence times of these back trajectories in the 100 m layer above the surface. Values above 0.001 p.p.m. μmol^{-1} m^{-2} s^{-1} comprise 97% of the land surface signal and values above 0.01 p.p.m. μmol^{-1} m^{-2} s^{-1} comprise 50% of the land surface signal; thus apparently small values are still important because they occupy a large area. Black arrows represent average climatological wind speed and direction in June, July and August (from the National Centers for Environmental Prediction (NCEP); http://www.esrl.noaa.gov/psd/data/gridded/data.ncep.reanalysis.html) averaged between the surface and 600 mbar. Open symbols (RPB and ASC) represent the NOAA tropical Atlantic sites used to define the background concentrations of CO_2, CO and SF_6 coming into the Amazon basin. Solid green dots indicate the locations of forest plot clusters where long-term biomass gains and respiration have been observed.

[1]Instituto de Pesquisas Energéticas e Nucleares (IPEN)–Comissao Nacional de Energia Nuclear (CNEN)–Atmospheric Chemistry Laboratory, 2242 Avenida Professor Lineu Prestes, Cidade Universitaria, Sao Paulo CEP 05508-000, Brazil. [2]School of Geography, University of Leeds, Woodhouse Lane, Leeds LS9 2JT, UK. [3]Global Monitoring Division, Earth System Research Laboratory, National Oceanic and Atmospheric Administration, 325 Broadway, Boulder, Colorado 80305, USA. [4]Cooperative Institute for Research in Environmental Sciences (CIRES), University of Colorado, Boulder, Colorado 80309, USA. [5]Environmental Change Institute, School of Geography and the Environment, University of Oxford, South Parks Road, Oxford OX1 3QY, UK. [6]Center for Weather Forecasts and Climate Studies, Instituto Nacional de Pesquisas Espaciais (INPE), Rodovia Dutra, km 39, Cachoeira Paulista CEP 12630-000, Brazil. [7]Remote Sensing Division, INPE (National Institute for Space Research), 1758 Avenida dos Astronautas, São José dos Campos CEP 12227-010, Brazil. [8]Departamento de Ciencias Atmosfericas/Instituto de Astronomia e Geofisica (IAG)/Universidade de Sao Paulo, 1226 Rua do Matao, Cidade Universitaria, Sao Paulo CEP 05508-090, Brazil. [9]Crew Building, The King's Buildings, West Mains Road, Edinburgh EH9 3JN, UK. [10]School of Tropical and Marine Biology and Centre for Terrestrial Environmental and Sustainability Sciences, James Cook University, Cairns 4870, Queensland, Australia. [11]Imperial College London, Silwood Park Campus, Buckhurst Road, Ascot SL5 7PY, Berkshire, UK.
*These authors contributed equally to this work.

in air at the other two sites, Alta Floresta (ALF) and Santarém (SAN) are not only from forests but also from savanna and agricultural land. Our measurements represent the first network of ongoing, well-calibrated CO_2 measurements over a large stretch of tropical land. Such measurements are vital, because the near-absence of CO_2 measurements sensitive to the tropical biosphere is the underlying cause of the large uncertainties in net flux estimates for tropical regions obtained by inverse modelling of atmospheric CO_2 (refs 14 and 15).

Fortuitously, the two years of atmospheric observations reported here are for an unusually dry year followed by a wet one (Fig. 2 and Extended Data Fig. 1a, b). Our measurements thus document the sensitivity of Amazon basin carbon pools to the effect of drought. The reasons for the dry conditions in 2010 were twofold. For the first three months an El Niño episode caused dry conditions in the north and centre of the Amazon basin, whereas during the second half of the year a positive North Atlantic sea surface temperature anomaly locked the inter-tropical convergence zone (where the northeast and southeast trade winds converge) into a position that was more northerly than usual. This caused enhanced and prolonged dry conditions in the southern areas of the Amazon basin (Extended Data Fig. 1a, b). A simple diagnostic of the stress on vegetation exerted by the negative precipitation anomalies is the climatological water deficit (CWD[16]; see Methods and Fig. 2), in which in 2010 large negative anomalies occurred for the northwestern basin. This is consistent with river discharge records[17]. Lesser negative anomalies in the northeastern basin were caused by early-year negative precipitation anomalies and the central–eastern and southern parts of the Amazon basin ('the arc of deforestation') had anomalies caused by low precipitation during the third quarter of the year. Monthly mean temperatures (Extended Data Fig. 1c, d) in 2010 were higher than average in every month, with especially large anomalies in February/March and August/September. These mirror the periods of greatest negative precipitation anomalies. Warmer than average temperatures (with respect to the last three decades) were also observed for every month of 2011, but 2011 was also an unusually wet year (Extended Data Fig. 1a, b). As shown below, observed basin-wide carbon flux variations for 2010 and 2011 reflect these temporal precipitation patterns.

To isolate the contribution of Amazon terrestrial carbon sources and sinks to the atmospheric CO_2 profiles, we first subtract a scalar background mole fraction from each of the observed profiles. This background

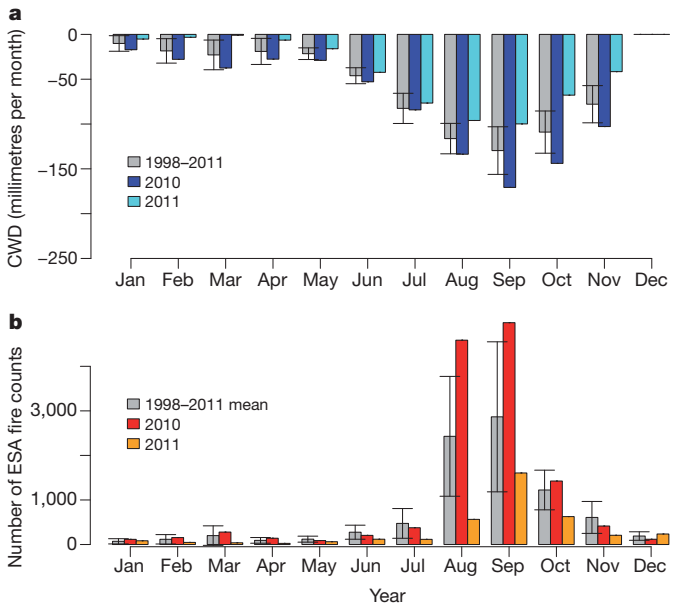

Figure 2 | Climatological water deficit. **a**, Basin-wide averages and standard deviation of CWD, based on the Tropical Rainfall Measuring Mission[28]. **b**, Fire counts based on European Space Agency (ESA; http://due.esrin.esa.int/wfa/) fire count data[29] for 2010, 2011 and 1998–2011, respectively.

represents the composition of air entering the Amazon basin from the Atlantic and is estimated as a weighted average of CO_2 at Ascension Island (ASC) and Ragged Point, Barbados (RPB) using a linear mixing model based on ASC and RPB SF_6 with weights determined from SF_6 measured at the site[18–20] (Methods). SF_6 is well suited for this purpose (that is, to estimate the fractional contributions of Northern and Southern Hemispheric air entering the basin) because it has a large inter-hemispheric difference (Extended Data Figure 8) and virtually no Amazonian emissions[21].

Carbon sources and sinks reveal themselves in the referenced profiles $\Delta X = X_{site} - X_{bg}$ as mole fraction enhancements and depletions, where X is the mole fraction of CO_2 or CO, for site and background. The enhancements and depletions are generally confined to the lowermost 2 km or so of the profiles (Fig. 3). For ΔCO_2 (Fig. 3a–d), there is a strong tendency towards surface enhancements during the dry season, although both lower-troposphere depletions and enhancements can be observed at any time of the year. Vertical profiles of ΔCO show very large enhancements above the Atlantic background in the dry season, persisting into the free troposphere (Fig. 3e–h and Extended Data Fig. 2). CO is a product of incomplete combustion and in the Amazon it reflects a contribution to CO_2 enhancements from biomass burning. This is confirmed by calculated air-mass back-trajectories intersecting satellite-sensed fire hotspots (Extended Data Fig. 3) and by our observed CO:CO_2 ratios, which are typical for those from tropical forest fires (Methods).

From the profiles of ΔX we estimate fluxes by dividing them by the air-mass travel time t from the coast to the sampling site and integrating from the surface (0 km above ground level, a.g.l.) to 4.4 km a.s.l. determined by air-mass back-trajectories calculated separately for each of (typically) 12 air samples per profile[18–20] to obtain:

$$F_X = \int_{z\ =\ 0\ \text{km (a.g.l.)}}^{4.4\ \text{km a.s.l.}} \frac{\Delta X}{t(z)} \mathrm{d}z \qquad (1)$$

Using measured CO:CO_2 emission ratios, $r^{bb}_{CO_2:CO}$ (refs 9 and 20), we further estimate the biomass burning contribution ($F^{bb}_{CO_2}$) to the net carbon flux using:

$$F^{bb}_{CO_2} = r^{bb}_{CO:CO_2}\left(F_{CO} - F^{bio}_{CO}\right) \qquad (2)$$

where F^{bio}_{CO} is the stable (background) value of F_{CO} during the wet season[20], reflecting direct plant and soil CO emissions as well as production from rapid oxidation of biogenic volatile organic compounds[22]. The non-fire net biome exchange (NBE) flux $F^{NBE}_{CO_2}$ is then given by:

$$F^{NBE}_{CO_2} = F^{total}_{CO_2} - F^{bb}_{CO_2} \qquad (3)$$

Our flux calculations (Fig. 4 and Table 1) reveal basin-wide average total fluxes of 0.19 ± 0.07 g C m^{-2} d^{-1} in 2010 and 0.02 ± 0.04 g C m^{-2} d^{-1} in 2011. Riverine carbon outgassing[13] is included in these fluxes but contributes minimally because the riverine organic carbon loop is very nearly closed within the Amazon basin[23], and fossil fuel emissions in the basin are negligibly small (<0.02 Pg C yr^{-1}; see Methods). Flux uncertainties presented in Fig. 4 and Table 1 may be underestimates because of losses of surface signal above 4.4 km caused by convective processes not captured by our extrapolation technique (Extended Data Table 1a). Our imperfect knowledge of convection and the difficulty of measuring CO_2 in the upper troposphere hamper quantification of these errors.

Using a basin area of 6.77×10^6 km^2 we calculate a source to the atmosphere of 0.48 ± 0.18 Pg C in 2010. In contrast, 2011 displayed an approximately neutral carbon balance (0.06 ± 0.10 Pg C yr^{-1}). In 2010, we calculate carbon losses due to fires of 0.51 ± 0.12 Pg C yr^{-1}, implying a carbon-neutral residual (that is, approximately zero NBE). On the other hand, for 2011 when NBE was -0.25 ± 0.14 Pg C yr^{-1}, the overall carbon balance was neutral, because this was offset by fire-associated losses of roughly the same size (0.30 ± 0.10 Pg C yr^{-1}). The return of

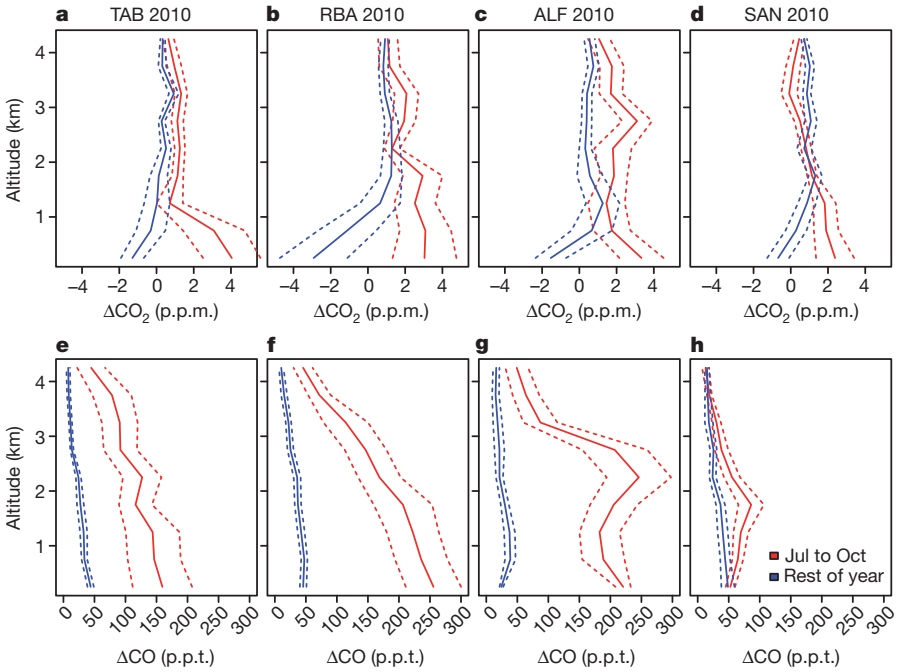

Figure 3 | Surface flux signals in vertical profiles. **a**–**d**, Mean difference between CO_2 profiles measured in 2010 at the four Amazonian aircraft sampling sites and oceanic CO_2 background (that is, ΔCO_2) during the dry (red lines) and wet (blue lines) seasons, respectively (solid lines) and the standard deviation divided by the square root of number of profiles (dashed lines). The background is estimated from in situ SF_6 and CO_2 at the NOAA/ESRL monitoring stations ASC and RPB, as described in the main text. **e**–**h**, As for **a**–**d**, but for CO. p.p.t., parts per trillion. The dry season (red lines) is affected by fires at most sites and is here defined as July–October for illustrative purposes only; it does not correspond to all months with fire emissions (see Methods).

the unburned Amazonian vegetation to being a sink in 2011 seems to have been driven primarily by precipitation, which changed from a negative anomaly in 2010 to a positive anomaly in 2011 (Extended Data Fig. 1a, b). However, temperatures were higher than average for both years, reflecting a net warming trend in recent decades (Extended Data Fig. 1c, d).

A more detailed picture of the Amazonian carbon cycle response to climate is revealed by the quarterly fluxes and by focusing first on RBA, TAB and ALF. For both years, during the first quarter of the year (the start of the wet season), measurements indicate a net carbon sink, and during the second and drier half of the year, measurements indicate a net source (Fig. 4a). However, during the second quarter of 2010 (in

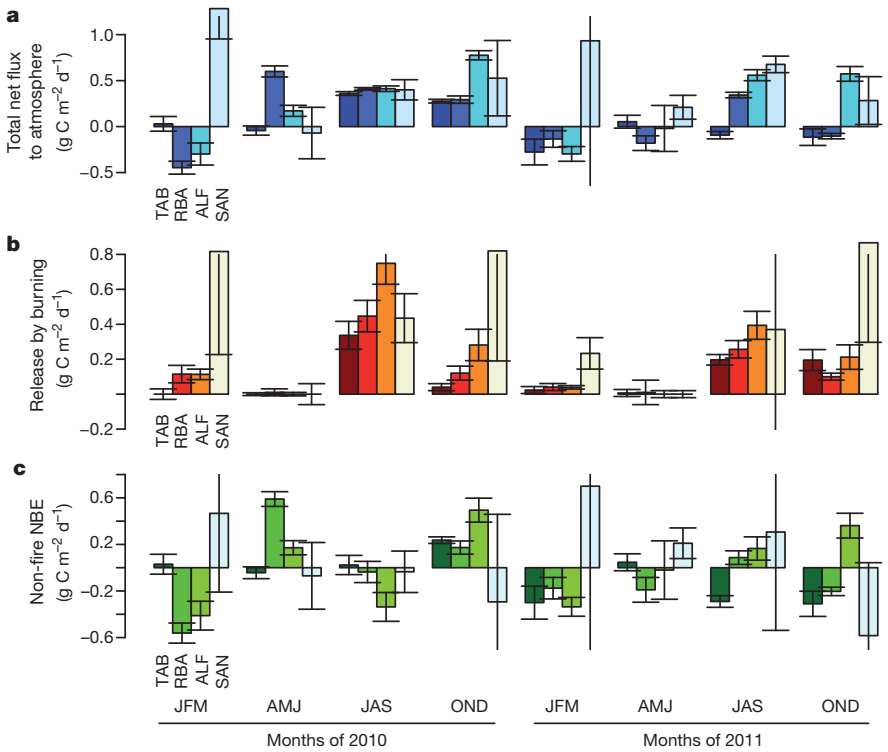

Figure 4 | Flux estimates summary. Quarterly flux and standard error (see Methods) of total carbon flux to the atmosphere (**a**), carbon release due to biomass burning (**b**) and carbon loss from the land (NBE) (**c**) based on the sites TAB, RBA, SAN and ALF for 2010 and 2011.

Table 1 | Summary of annual carbon flux estimates

Sites	TAB	RBA	SAN	ALF	
	2010 fluxes ($g C m^{-2} d^{-1}$)				Scaled 2010 flux ($Pg C yr^{-1}$)†
Total	0.15 ± 0.10	0.17 ± 0.11	0.33 ± 0.50	0.29 ± 0.15	0.48 ± 0.18
Fire	0.13 ± 0.05	0.17 ± 0.06	0.57 ± 0.45	0.28 ± 0.09	0.51 ± 0.12
NBE	0.02 ± 0.11	0.00 ± 0.13	−0.25 ± 0.70	0.01 ± 0.17	−0.03 ± 0.22
	2011 fluxes ($g C m^{-2} d^{-1}$)				Scaled 2011 flux ($Pg C yr^{-1}$)†
Total	−0.10 ± 0.07	−0.04 ± 0.07	0.46 ± 0.20	0.24 ± 0.06	0.06 ± 0.10
Fire	0.08 ± 0.03	0.09 ± 0.03	0.44 ± 0.51	0.16 ± 0.04	0.30 ± 0.10
NBE	−0.18 ± 0.08	−0.13 ± 0.08	0.02 ± 0.84	0.08 ± 0.07	−0.25 ± 0.14
Area of influence ($\times 10^6 km^2$)*	2.53	3.67	0.59	1.31	

The uncertainties are standard errors calculated by propagating uncertainties in all equations using a Monte Carlo approach, and then taking half the value of the 16th–84th percentile range. A bootstrapping approach to calculate the standard error (2.5th–97.5th percentile range) yields slightly smaller values.
* Back-trajectory ensemble envelope (that is, the total area of influence of a measuring site as estimated from wind back-trajectory ensembles).
† 'Scaled' means the flux estimates have been scaled to the tropical South America forested area, assuming an Amazon forest area of $6.77 \times 10^6 km^2$ (ref. 30).

contrast to 2011) we calculate the flux to be a carbon source, which slightly lags the strong precipitation and temperature anomalies in February and March. Net emissions during the second half of 2010 were more than twice as large as in 2011, corresponding to precipitation and temperature anomalies in August and September 2010. For both years, however, the difference in carbon release between the second and first half of the year is mainly due to fire emissions (Fig. 4 and Extended Data Fig. 2). The larger fire emissions in 2010 are consistent with the anomalously high fire counts observed from space (Fig. 2b, Extended Data Figure 2) and basin-wide CO anomalies, which in 2010 extended well above ~2 km a.s.l. (roughly the planetary boundary layer height) into the free troposphere, even at the more remote sites RBA and TAB (Fig. 3e–h and Extended Data Fig. 2). Moreover, the 'arc of deforestation' in the southern and eastern Amazon basin was one of the regions with the strongest precipitation anomalies (Extended Data Fig. 1a, b), intensifying the meteorological conditions required for fire ignition and persistence, and probably leading to the large burning emissions we observed in 2010. After accounting for fire emissions, the residual NBE reveals large differences between the years, especially for the second and fourth quarters, for which there were large carbon releases in 2010 but smaller ones in 2011. This difference in seasonality between the two years appears to reflect a lagged drought stress induced by precipitation anomalies in February/March (first quarter) and August/September (third quarter) of 2010.

The fluxes calculated from the SAN data differ from the other three sites both in seasonality and in the contrast between 2010 and 2011, with a strong carbon source in the first quarter of the year for air sampled upwind of SAN (but not the other three sites) especially notable. This may result in part from the fire season extending into January for the eastern Amazon and northeast Brazil, which is not the case for the moister central/western areas. Additionally, eddy-flux data[11] and CO_2 vertical profile analysis[20] show that (unburned) forests in the eastern Amazon are net sinks in the dry season and net sources in the wet season. In contrast, other sites tend to show wet season uptake (Figs 3a–d and 4).

Additional insight about the cause of the difference in 2010 and 2011 NBE comes from observations at a network of 14 intensive forest carbon cycle measurement plots established across the Amazon basin. At these plots a near-complete suite of carbon pools is being observed, providing an estimate of net primary production and autotrophic respiration and thus an upper bound on gross primary production[5]. Six of these plots experienced anomalous drought stress in 2010, at which time gross primary production declined (Extended Data Fig. 5a), and there were minimal positive temperature anomalies (Extended Data Fig. 5b). Combined, atmospheric mass balance and forest plot analysis suggest that drought has an important negative effect on Amazon forest productivity and with likely consequences on future changes in the forests. This is in contrast to a recent analysis of future Amazon carbon losses calibrated via inter-annual responses of global atmospheric CO_2 growth rates to tropical temperature anomalies[24].

Tropical temperature anomalies have tended to covary with moisture anomalies in the past, so although these models seem to reproduce recent variability correctly they may do so for the wrong reason. Moreover, as 2011 shows, positive temperature anomalies can also coincide with non-drought years.

Besides the new insights into large-scale controls of carbon pool responses in a changing climate, our results provide a top-down confirmation that during non-drought years intact Amazonian forests are a substantial carbon sink, consistent with theoretical predictions for forest biomass alone[25]. Our NBE estimate for 2011 is smaller than the mean annual biomass sink of 0.39 ± 0.10 Pg C estimated for the 1980–2004 period based on repeated censuses at a widespread forest plot network[7]. However, our fire flux estimate is not identical to the total deforestation emissions, which includes emissions from heterotrophic respiration, thus slightly biasing our NBE estimate. The Deforestation Carbon Flux (DECAF) land-use change model[26] suggests that the sources of deforestation emissions in the southern Amazon are typically 30% respiration and 70% fire, implying 2011 deforestation fluxes of about $+0.4\ Pg\ C\ yr^{-1}$, and therefore NBE of about $-0.4\ Pg\ C\ yr^{-1}$, closing the gap between the top-down and bottom-up estimates. In 2011 in particular, respiration could have been stimulated following enhanced tree mortality caused by the 2010 drought[27].

In summary, we have empirically documented a pronounced response of a large fraction of the Amazonian vegetation to drought, with forest productivity stalled and large amounts of carbon released by fire in 2010. The Amazon basin returned to being a net carbon sink in 2011. But our results are cause for concern in the light of the recent increase in precipitation extremes and increasing temperatures. If these climate trends continue, future shifts in Amazon forest function, leading to reduced carbon uptake, are likely. This could exacerbate carbon losses as a result of direct human activities such as deforestation.

METHODS SUMMARY

Air sample profiles were taken using small aircraft descending in a spiral from approximately 4,420 m to about 300 m a.s.l. (as close to the forest canopy as possible), semi-automatically filling 12 (for the TAB, ALF and RBA sites) and 17 (for the SAN site) 0.7-litre flasks controlled from a microprocessor and contained in one suitcase. Profiles are taken between 12:00 and 13:00 local time. At that time, the boundary layer is close to being fully developed. Once a vertical profile has been sampled (one suitcase filled) it is transported to the IPEN Atmospheric Chemistry Laboratory in Sao Paulo, where samples are analysed by a replica of the NOAA/ESRL trace gas analysis system. All aircraft data used in this study is available at ftp://ftppub.ipen.br/nature_gatti_etal/. The accuracy and precision of the system are evaluated with three independent procedures that demonstrate excellent performance with long-term repeatability (1σ) of ±0.03 parts per million (p.p.m.) and a difference between measured and calibrated values of 0.03 p.p.m. Because NOAA/ESRL Atlantic data from the ASC and RPB sites are used as background values for Amazonian measurements made at IPEN, this high accuracy is required to ensure that spatial gradients are not artefacts of calibration. The CO and SF_6 measurements presented here are also made at IPEN with calibration standards

tied directly to the World Meteorological Organization reference scales maintained by NOAA/ESRL.

Online Content Any additional Methods, Extended Data display items and Source Data are available in the online version of the paper; references unique to these sections appear only in the online paper.

Received 24 May; accepted 12 December 2013.

1. Huntingford, C. *et al.* Contributions of carbon cycle uncertainty to future climate projection spread. *Tellus B* **61,** 355–360 (2009).
2. Friedlingstein, P. *et al.* Climate-carbon cycle feedback analysis: results from the (CMIP)-M-4 model intercomparison. *J. Clim.* **19,** 3337–3353 (2006).
3. Phillips, O. L. *et al.* Changes in the carbon balance of tropical forests: evidence from long-term plots. *Science* **282,** 439–442 (1998).
4. Huntingford, C. *et al.* Simulated resilience of tropical rainforests to CO_2-induced climate change. *Nature Geosci.* **6,** 268–273 (2013).
5. Malhi, Y. *et al.* The regional variation of aboveground live biomass in old-growth Amazonian forests. *Glob. Change Biol.* **12,** 1107–1138 (2006).
6. Gloor, M. *et al.* Intensification of the Amazon hydrological cycle over the last two decades. *Geophys. Res. Lett.* **40,** 1729–1733 (2013).
7. Phillips, O. L. *et al.* Drought sensitivity of the Amazon rainforest. *Science* **323,** 1344–1347 (2009).
8. Lloyd, J. *et al.* An airborne regional carbon balance for Central Amazonia. *Biogeosciences* **4,** 759–768 (2007).
9. Chou, W. W. *et al.* Net fluxes of CO_2 in Amazonia derived from aircraft observations. *J. Geophys. Res.* **107,** 4614, http://dx.doi.org/10.1029/2001JD001295 (2002).
10. Saleska, S., da Rocha, H. R. & Nobre, A. in *Amazonia and Global Change Geophysical Monograph Series* **186,** 389–407 (ed. Gash, J., Keller, M. & Silva Dias, P.) (American Geophysical Union, 2009).
11. Saleska, S. R. *et al.* Carbon in Amazon forests: unexpected seasonal fluxes and disturbance-induced losses. *Science* **302,** 1554–1557 (2003).
12. Houghton, R. A. Revised estimates of the annual net flux of carbon to the atmosphere from changes in land use and land management 1850–2000. *Tellus B* **55,** 378–390 (2003).
13. Richey, J. E., Melack, J. M., Aufdenkampe, A. K., Ballester, V. M. & Hess, L. L. Outgassing from Amazonian rivers and wetlands as a large tropical source of atmospheric CO_2. *Nature* **416,** 617–620 (2002).
14. Gurney, K. R. *et al.* Towards robust regional estimates of CO_2 sources and sinks using atmospheric transport models. *Nature* **415,** 626 (2002).
15. Stephens, B. B. *et al.* Weak northern and strong tropical land carbon uptake from vertical profiles of atmospheric CO_2. *Science* **316,** 1732–1735 (2007).
16. Aragão, L. E. O. C. *et al.* Spatial patterns and fire response of recent Amazonian droughts. *Geophys. Res. Lett.* **34,** L07701, http://dx.doi.org/10.1029/2006gl028946 (2007).
17. Espinoza, J. C. *et al.* Climate variability and extreme drought in the upper Solimões River (western Amazon Basin): understanding the exceptional 2010 drought. *Geophys. Res. Lett.* **38,** L13406, http://dx.doi.org/10.1029/2011gl047862 (2011).
18. Miller, J. B. *et al.* Airborne measurements indicate large methane emissions from the eastern Amazon basin. *Geophys. Res. Lett.* 34, L10809, http://dx.doi.org/10.1029/2006GL029213 (2007).
19. D'Amelio, M. T. S., Gatti, L. V., Miller, J. B. & Tans, P. Regional N_2O fluxes in Amazonia derived from aircraft vertical profiles. *Atmos. Chem. Phys.* **9,** 8785–8797 (2009).
20. Gatti, L. V. *et al.* Vertical profiles of CO_2 above eastern Amazonia suggest a net carbon flux to the atmosphere and balanced biosphere between 2000 and 2009. *Tellus B* **62,** 581–594 (2010).
21. European Commission. Emission Database for Global Atmospheric Research (EDGAR) version 4.0, http://edgar.jrc.ec.europa.eu/overview.php?v=40 (Joint Research Centre/Netherlands Environmental Assessment Agency, 2009).
22. Greenberg, J. P. *et al.* Biogenic VOC emissions from forested Amazonian landscapes. *Glob. Change Biol.* **10,** 651–662 (2004).
23. Gloor, M. *et al.* The carbon balance of South America: a review of the status, decadal trends and main determinants. *Biogeosciences* **9,** 5407–5430 (2012).
24. Cox, P. M, *et al.* Sensitivity of tropical carbon to climate change constrained by carbon dioxide variability. *Nature* **494,** 341–344 (2013).
25. Lloyd, J. & Farquhar, G. D. The CO_2 dependence of photosynthesis, plant growth responses to elevated atmospheric CO_2 concentrations and their interaction with soil nutrient status. I. General principles and forest ecosystems. *Funct. Ecol.* **10,** 4–32 (1996).
26. van der Werf, G. R. *et al.* Estimates of fire emissions from an active deforestation region in the southern Amazon based on satellite data and biogeochemical modelling. *Biogeosciences* **6,** 235–249 (2009).
27. Lewis, S. L., Brando, P. M., Phillips, O. L., van der Heijden, G. M. F. & Nepstad, D. The 2010 Amazon drought. *Science* **331,** 554 (2011).
28. Liu, Z., Ostrenga, D., Teng, W. & Kempler, S. Tropical Rainfall Measuring Mission (TRMM) precipitation data and services for research and applications. *Bull. Am. Meteorol. Soc.* **93,** 1317–1325 (2012).
29. Arino, O., Casadio, S. & Serpe, D. Global night-time fire season timing and fire count trends using the ATSR instrument series. *Remote Sens. Environ.* **116,** 226–238 (2012).
30. INPE. *PRODES (Projeto de Deflorestamento da Amazônia)* http://www.obt.inpe.br/prodes/index.html (2011).

Acknowledgements We thank P. Tans and P. Bakwin, who had the foresight to initiate a long-term high-precision greenhouse gas measurement laboratory in Sao Paulo, and D. Wickland, the NASA programme manager who initially supported this effort. This work has been financed primarily by the UK Environmental Research Council (NERC) via the consortium grant 'AMAZONICA' NERC (NE/F005806/1) and also by the State of Sao Paulo Science Foundation (FAPESP) via the 'Carbon Tracker' project (08/58120-3), and the EU via the 7th grant framework GEOCARBON project (grant number agreement 283080). NASA, NOAA and IPEN made large contributions to the construction and maintenance of the GHG laboratory in Brazil. Intensive plot measurements were supported by NERC and the Moore Foundation via grants given to RAINFOR. L.G.D., L.S.B., C.S.S.C., V.F.B. and A.M. were supported by CNPq, CAPES, Fapesp and IPEN, and O.L.P. by an ERC Advanced Grant. We thank measurement analysts and scientists at NOAA for providing data, and the pilots who collected the air samples. Numerous people at NOAA, especially A. Crotwell, D. Guenther, C. Sweeney and K. Thoning, provided advice and technical support for air sampling and measurements in Brazil. E. Dlugokencky provided data from Ascension Island and Ragged Point in Barbados. We also thank D. Galbraith for help with the comprehensive forest census plot data and R. Brienen for comments. Finally, we acknowledge S. Denning for reviews of the manuscript.

Author Contributions L.V.G., M.G., J.B.M., J.L., H.R., O.L.P., Y.M. and J.G. conceived the basin-wide measurement programme and approach. M.G., J.B.M. and L.V.G. wrote the paper. C.E.D. and Y.M. analysed and contributed the data of the comprehensive biometric forests census plots. S.F., R.B., L.O.A., L.G.D. and L.S.B. helped with data analysis. V.F.B., C.S.C.C. and A.M. helped with greenhouse gas concentration analysis. All co-authors commented on the manuscript.

Author Information Reprints and permissions information is available at www.nature.com/reprints. The authors declare no competing financial interests. Readers are welcome to comment on the online version of the paper. Correspondence and requests for materials should be addressed to L.V.G. (lvgatti@gmail.com), M.G. (eugloor@gmail.com) and J.B.M. (john.b.miller@noaa.gov).

METHODS

Air sampling and analysis. Air is sampled by semi-automatic filling of borosilicate flasks stored inside purpose-built suitcases (called 'programmable flask packages'), which contain an array of 17 0.7-litre flasks at SAN site and 12 0.7-litre flasks at TAB, ALF and RBA. The programmable flask packages are connected to a second suitcase containing batteries and two compressors in series (called 'programmable compressor packages'), which is connected to an air inlet on the outside of the aircraft. More details of these packages are available at http://www.esrl.noaa.gov/gmd/ccgg/aircraft/sampling.html.

To fill the flasks at our set of pre-determined altitudes, the aircraft pilot initiates sampling by toggling a switch that initiates the pumps in the programmable compressor package and switches flask valves in the programmable flask package. Its manifold is first flushed with 5 litres of air, and then the flask valves are opened and flushed with 10 litres of air. The downstream flask valve is then closed and the samples are pressurized to 260 kPa before closing the upstream valve. The full set of 12 or 17 flasks are filled during one descending spiral profile from 4,420 m to 300 m a.s.l. From altitudes of 4,420 m down to 1,200 m we sampled every 300 m and from 1,200 m downwards we sampled every 150 m down to almost the canopy. Profiles were usually taken between 12:00 and 13:00 local time, because this is the time when the boundary layer is close to being fully developed. It is also the time at which the column average is most similar to the daily mean[9].

Once a programmable flask package (that is, one vertical profile) has been filled with air, it is transported to the IPEN Atmospheric Chemistry Laboratory in Sao Paulo, where it is analysed by a replica of the NOAA/ESRL/GMD trace gas analysis system at Boulder, Colorado, USA. Air samples are analysed for CO_2, CO and SF_6 (as well as CH_4, N_2O and H_2). CO_2 is measured with a non-dispersive infrared analyser[20], CO by gas chromatography followed by HgO reduction detection and SF_6 by gas chromatography followed by electron capture detection. Reference gases for all species were obtained from NOAA/ESRL and are directly tied to the World Meteorological Organization official standard scales.

Once analysed, the flasks are prepared for sampling by flushing them with dry air, followed by synthetic air with 350 p.p.m. CO_2. Because our approach depends on CO_2, CO and SF_6 measurements from both the IPEN (aircraft-based vertical profiles) and NOAA/ESRL laboratories (background site records at RPB and ASC) high accuracy ('measurement trueness') is crucial. The procedures followed to ensure high accuracy have been documented in ref. 20. Three methods of assessing inter-laboratory comparability are being routinely pursued. First, comparisons of CO_2 mole fraction from 'target tanks' (calibrated air cylinders treated as unknowns) demonstrate the long-term repeatability (standard deviation, 1σ, of 20 analyses) of $\pm$0.03 p.p.m. (here 'long-term repeatability' refers to our estimate of the stability of our implementation of the calibration scale at the IPEN laboratory over 5–10 years) and a difference between measured and calibrated values of 0.03 p.p.m. (the calibrated mole fraction at NOAA/ESRL was 378.60 $\pm$ 0.03 p.p.m. and at IPEN it was 378.57 $\pm$ 0.03 p.p.m.). Second, a comparison of air in flask pairs sampled weekly by IPEN and NOAA/ESRL (pairs taken within 20–30 min of each other) on the Atlantic coast and analysed by NOAA/ESRL and IPEN has been in operation since October 2006. Weekly samples have been collected at Arembepe, Bahia (2006–2010) and Natal, Rio Grande do Norte (2010 to present). Results show a mean difference of only +0.02 p.p.m. (IPEN minus NOAA). Finally, the international 5th World Meteorological Organization RoundRobin[31] in which three target tanks were measured by numerous laboratories around the world showed differences between IPEN and the calibrated value of only +0.02–0.03 p.p.m.

Sampling sites and regions of influence. Extended Data Fig. 6a shows the 2010 surface sensitivities ('footprints') of each of the four aircraft sites in the annual average as simulated by the FLEXPART Lagrangian particle dispersion model[32]. The footprints are calculated by simulating the backwards-in-time transport of 10,000 infinitesimal air 'particles' for 7–14 days and registering their intersection with a 100-m layer above the surface. The driving meteorology used is from the NCEP Global Forecast System with a resolution of $0.5^\circ \times 0.5^\circ$. To generate each panel in Extended Data Fig. 6a, footprints were calculated for each sample at the appropriate time and location and then averaged over the entire year. Although the near-surface samples (0–1,500 m a.s.l.) contribute disproportionately to the full-profile average, the free troposphere footprints contribute significantly to the total (unlike in the mid-latitudes), probably because of enhanced convection.

Comparing Extended Data Fig. 7a, b with the average footprints in Extended Data Fig. 6a allows us to understand the ecosystems that are influencing observations at each site. Extended Data Fig. 6b shows just the portion of the average footprints in each site that is co-incident with the tropical forest biome shown in Extended Data Fig. 7a. Sites RBA and TAB show a 20% reduction in integrated surface sensitivity when considering just tropical forest, while ALF and SAN show more than a 40% reduction in integrated surface sensitivity. The non-forest biomes that influence our measurements are primarily savannas (the Cerrado south of the tropical forest region and the Caatinga along the northeast coast of Brazil, which are both classified as savanna in Extended Data Fig. 7a) and grasslands to a lesser extent. Although not shown by the biome map (Extended Data Fig. 7a), our study area also includes two major cities, Belem (2.5 million people) in the state of Para, near the mouth of the Amazon, and Manaus (2.3 million people) at the confluence of the Negro and Solimões (Amazon) rivers. However, convolution of the average footprints at each site with monthly fossil fuel emission fields (with internal national patterns based on location of power plants and population density; see http://www.esrl.noaa.gov/gmd/ccgg/carbontracker/documentation_ff.html#ct_doc) show that the Belem and Manaus emissions contribute only about 0.01–0.03 p.p.m. to each observation. Overall, the fossil fuel flux for the basin based on the inventory we use is less than 0.02 Pg C yr^{-1}.

Flux estimation. As described in the main text, we calculate individual fluxes from the difference of site vertical profiles and corresponding background values and the travel time of air parcels along the trajectory from the coast to the site (equation (1)). To apply equation (1) we convert mole fractions (μmol CO_2 per mole dry air, that is, p.p.m.) to concentrations (moles CO_2 per cubic metre) using observed lapse rates and an exponentially declining air column pressure profile with a scale height H of 7 km, that is, $p(z) = p(0)\exp(-z/H)$. For assigning background concentrations we assume well-mixed vertical profiles at ASC and RPB, which is supported by the profiles measured in 2000–2003 at the coastal site Fortaleza[20].

We estimate the background CO_2 concentration from SF_6 measured at the site and the NOAA/ESRL background observation sites RPB and ASC, respectively (Extended Data Fig. 8b). Background CO_2 values are calculated using a linear mixing model and smoothed representations of the CO_2 (or CO) time series at RPB and ASC (Extended Data Fig. 8b)[18] as

$$X_{bg} = f^{ASC}X^{ASC} + \left(1 - f^{ASC}\right)X^{RPB} \quad (4)$$

with

$$f^{ASC} = \frac{SF_6^{site} - SF_6^{RPB}}{SF_6^{ASC} - SF_6^{RPB}} \quad (5)$$

f_{ASC} is the fraction of air arriving at the site originating from the latitude of ASC and SF_6^{site} is the median SF_6 value from the SAN vertical profile. SF_6^{ASC} or SF_6^{RPB} is the SF_6 mole fraction extracted from a smoothed curve fit[33] to the SF_6 record of ASC or RPB from n days before a given vertical profile at the site (where $n = 4$ for SAN, $n = 7$ for ALF, $n = 8$ for TAB and $n = 9$ for RBA). X refers to the mole fraction of any gas co-measured with SF_6; in this case, CO_2 and CO. We bound f^{ASC} and f^{RPB} at 0 and 1. This algorithm assumes that the SF_6, CO_2 and CO meridional gradients in the tropical Atlantic are linear between about 18° S and 23° N (although values of f^{RPB} rarely exceed 0.5, meaning that the northern linearity criterion need only be met to 13° N, the latitude of RPB). This linearity requirement is accurate in general, but deviations from it contribute to uncertainty in our flux calculation. The bounds we place on f^{ASC} and f^{RPB} reflect caution in assuming linearity much further to the north or south of our background sites; when f^{ASC} and f^{RPB} exceed the bounds, we use values of 0 and 1.0. We assume the background profile, entering from the oceans, to be well mixed vertically. Our background calculation based on SF_6 and the NOAA/ESRL station records at Barbados and Ascension assumes that ocean outgassing/uptake along air parcels travelling from somewhere on the line between RPC and ASC is negligible (Extended Data Fig. 7a). The differences between our calculated background based on the RPC and ASC sites and actual measurements at Maxaranguape/Natal (site code NAT, 15 m a.s.l., 5° 29′ 22″ S, 35° 15′ 40″ W) are very small and thus confirm this assumption. This site is located 50 km north of the Natal city, located on the Atlantic coast of Brazil.

To estimate travel times (that is, the denominator, t, of equation (1)), we calculate back trajectories for each air sampling level. 14-day backwards trajectories are derived from the online version of the HYSPLIT model[34] for each sample altitude (for each sampling day). Then, with a resolution of 3 h, the time when the back trajectory crosses the coast is calculated. In a small number of cases (~5%), the trajectory is 'trapped' on land, even after 14 days. In these cases, t is assigned a value of 14 days. The sensitivity of the flux estimates to the back-trajectory calculation is shown in Extended Data Table 1b and discussed below. Mean travel times from the coast to SAN, ALF, TAB and RBA were 2.6 days, 5.0 days, 6.8 days and 7.7 days respectively. For each height interval, we calculate the associated flux and then sum them to obtain the flux estimate for the specific measured profile. For calculating annual means, we first calculate monthly mean fluxes (with number of fluxes per site per month being typically two) and then average them.

To estimate fluxes due to fire using equation (2) we estimate CO:CO_2 fire emission ratios, $r^{bb}_{CO_2:CO}$, from clearly identifiable plumes in our data. We also use months with identifiable fire plumes to define in which months we subtract fire emissions. For 2010, this period was January, February and July–December at all sites. For 2011, these months were July–December for TAB; February and August–December for RBA; January, February and July–December for SAN; and July–December for ALF.

For calculating annual means, we first calculate monthly mean fluxes (with number of fluxes per site per month being typically two) and then average.

Uncertainty analysis. To assess the uncertainty of our approach we use both formal error propagation with Monte Carlo randomization of all parameters as well as a set of sensitivity calculations in which we change assumptions used in our calculations (see below).

Monte Carlo error propagation. For Monte Carlo error propagation we take into account the uncertainty in the background concentration and the uncertainty in air parcel travel time, and for separation of total fluxes in fire and land vegetation fluxes unrelated to fire, we account for the uncertainty in emission ratios.

The uncertainty due to CO_2 measurement uncertainty (<0.1 p.p.m.) is negligibly small. However, in the calculation of the background values, we do account for the more significant (~0.5%) measurement uncertainty for SF_6. We assume uncertainties of back-trajectory travel times to be normally distributed with a standard deviation of $\sigma = 0.5$ day for SAN and $\sigma = 1$ day for RBA, TAB and ALF. Uncertainties of background mole fractions X_{bg} (equation (4)) vary seasonally and are derived by propagating the 0.5% uncertainty in median SF_6 values in equation (5) into equation (5), where uncertainties from X_{ASC} and X_{RPB} come from the standard deviation of the residuals to curve fits[33] (using a short-term residuals smoother of about 150 days) to CO_2 and SF_6 observations. Uncertainties in X_{bg} vary seasonally as the CO_2 seasonal cycles for ASC and RPB converge (lower uncertainty in X_{bg}) and diverge (higher uncertainty in X_{bg}) as can be seen in Extended Data Fig. 8a, b. For each set of randomly perturbed profiles for the year 2010 an annual mean flux is calculated. Annual mean flux distributions from these calculations are shown for each site in Extended Data Fig. 4b.

We have also used bootstrapping to estimate uncertainties, for which 95% confidence intervals are slightly smaller than the uncertainty estimates (16%–84% spread in distribution calculated using Monte Carlo randomization). We present the larger of these in Table 1.

Sensitivity of results to assumptions used to estimate fluxes. Sensitivity calculations focus on two factors: the travel time of air parcels from the Atlantic coast to the site and the flux signal above 4.4 km a.s.l.

In addition to using HYPSLIT[34], as we do for the calculation in the main text, we test the sensitivity of our travel times (only in 2010) by using those derived from the FLEXPART Lagrangian particle dispersion model[32] and back trajectories derived from the meso-scale model B-RAMS[35]. The sensitivity calculation here is simplified with respect to the calculation of fluxes in the main text in that we divide the profile into three equal-altitude segments and use average travel times for each segment. Extended Data Table 1b shows that differences in annual mean fluxes calculated using the three different sets of modelled travel times (relative to that of FLEXPART) are always less than 0.1 g C m^{-2} d^{-1} and are typically much smaller than this. Significantly, the relative magnitudes between sites are not sensitive to changes in the model.

To assess our assumption that we can neglect the portion of vertical profiles above 4.4 km, we extend each vertical CO_2 profile linearly up to 8 km, 10 km or 12 km a.s.l. converging to a mole fraction equal to the background value (that is, $\Delta CO_2 = 0$). In the annual mean, increasing the height of the column integrals increases the size of the calculated source flux at all sites except TAB, by an average of about 0.1 g C m^{-2} d^{-1}; at TAB there is no significant impact of increasing the integration height (Extended Data Table 1b and Extended Data Fig. 4a). Seasonally there are both increases and decreases in flux, but in all cases, seasonal sources and sinks both become slightly stronger when increasing the integration height (Extended Data Table 1a).

Scaling to the basin. We scale our estimates in two ways. First, we weight annual flux estimates f_i derived from each of the station records separately by the station's footprint area A_i as:

$$F = \bar{f} A_{forests} \tag{6}$$

where

$$\bar{f} = \left(\sum_{i=1}^{4} A_i f_i \right) / \sum_{i=1}^{4} A_i$$

and the Amazon forested area $A_{forests} = 6.77 \times 10^6$ km^2 (ref. 30) and propagate errors accordingly, and second, we treat our flux estimates as independent estimates of the same quantity and combine errors accordingly.

Climatological water deficit. CWD[16] is calculated recursively as $CWD_{n+1} = CWD_n + P - E_0$ where P is precipitation, $E_0 = 0.1$ m per month is an estimate of the average monthly evaporation of an intact forest and n is the number of the month following the wettest month. CWD is set to zero in October, reflecting soil water recharge at the height of the rainy season.

Full carbon accounting at intensive forest census plots. Comprehensive carbon cycle sites provide bottom-up estimates of net primary productivity (NPP) and autotrophic respiration terms (R_{auto}) by quantifying individual components of the carbon cycle independently. The major NPP components measured include leaf production (taken to be equivalent to leaf litterfall over an annual cycle), stem production (based on measurements of stem diameter growth) and fine root production (based on measurements of ingrowth cores). Major autotrophic respiration components (leaf respiration, stem respiration and root respiration) are measured as well. Gross primary production is estimated to equal plant carbon expenditure (PCE) or the sum of total NPP and autotrophic respiration over long periods (about a year). Most NPP and respiration components were measured on a monthly basis, but some components (root productivity and leaf respiration) were measured at coarser time intervals.

Measurements were distributed evenly through the plot, approximately one per subplot (except for the 16 ingrowth cores, which were at the corners of subplots). A detailed description of all measurements is available online for download (http://gem.tropicalforests.ox.ac.uk). Detailed information on the methodology and graphs showing data from each individual component from all sites are available from a series of companion papers (measurements for 2009–2010)[36–44]:

$$R_{auto} = R_{canopy} + R_{woody} + R_{rhizosphere} \tag{7}$$

$$NPP_{total} = NPP_{wood} + NPP_{canopy} + NPP_{fineroots} \tag{8}$$

$$PCE = NPP_{total} + R_{auto} \tag{9}$$

In the above equations, R represents different components of autotrophic respiration and NPP are different components of growth. To calculate PCE, we use the above equations, which differ slightly from previous calculations in that they do not include some of the more minor components because they are not measured with as high a temporal resolution. For the droughted sites we processed an additional year of our data (2011; this work).

Results from intensive carbon cycle measurement plots. Local meteorological stations within 1 km of the intensive forest plots indicate that the drought at the sites listed in Extended Data Fig. 5c occurred approximately between May and December 2010 (box marked drought in Extended Data Fig. 5a). Plant carbon expenditure (PCE) for eight 1-hectare plots show few average differences between 2009 and 2010 (blue line). The three humid tropical droughted plots (black line) show a deviation in PCE during the drought period from the 2009 average (black dashed line). This lasted for approximately the whole drought and returned to the 2009 average in later 2011. The three droughted plots in the dry margins of Amazonia (red line) showed decreased PCE that extended into 2011, indicating a larger effect of the drought in drier regions. However, the dry margins make up only the extremities of the Amazon basin.

Thus, humid tropical forests decreased PCE during the drought period. We estimate that changes in PCE would lag changes in gross primary production because the plants can initially depend on non-structural carbohydrate energy stores. Therefore, any decrease in photosynthesis would have been before the decrease in PCE, consistent with the atmospheric measurement analysis.

We also analysed temperature data at these sites (Extended Data Fig. 5b). For the drought plots, the start of 2010 was warmer than average, but during most of the drought period (based on CWD) temperatures were near the average at the intensive forest plots. 2011 had slightly above average temperatures for the drought plots over the entire year. Therefore, our drought plots experienced greater moisture stress in 2010 versus 2011, but the temperature stress in both years was similar.

31. Zhou, L. X., Kitzis, D. & Tans, P. in *Report of the Fourteenth WMO/IAEA Meeting of Experts on Carbon Dioxide Concentration and Related Tracer Measurement Techniques* Vol. 186 40–43 (WMO/Global Atmospheric Watch, 2009).
32. Stohl, A., Forster, C., Frank, A., Seibert, P. & Wotawa, G. The Lagrangian particle dispersion model FLEXPART version 6.2. *Atmos. Chem. Phys.* **5,** 2461–2474 (2005).
33. Thoning, K. W., Tans, P. P. & Komhyr, W. D. Atmospheric carbon dioxide at Mauna Loa Observatory 2. Analysis of the NOAA GMCC data, 1974-1985. *J. Geophys. Res.* **94,** 8549–8565 (1989).
34. Draxler, R. R. & Rolph, G. D. *HYSPLIT (HYbrid Single-Particle Lagrangian Integrated Trajectory)* http://ready.arl.noaa.gov/HYSPLIT.php (NOAA, 2013).
35. Freitas, S. R. *et al.* The Coupled Aerosol and Tracer Transport model to the Brazilian developments on the Regional Atmospheric Modeling System (CATT-BRAMS)—Part 1: Model description and evaluation. *Atmos. Chem. Phys.* **9,** 2843–2861 (2009).
36. del Aguila-Pasquel, J. *et al.* The seasonal cycle of productivity, metabolism and carbon dynamics in a wet aseasonal forest in NW Amazonia (Iquitos, Peru). *Plant Ecol. Divers.* **7,** 71–83 (2013).
37. Araujo-Murakami, A. *et al.* The productivity, allocation and cycling of carbon at the dry margin of the Amazon forest in Bolivia. *Plant Ecol. Divers.* **7,** 55–69 (2013).

38. da Costa, A. *et al.* Seasonality of ecosystem respiration and net primary productivity after 8–10 years of experimental drought in an eastern Amazon forest. *Plant Ecol. Divers.* **7,** 7–24 (2013).
39. Doughty, C. E. *et al.* The production, allocation and cycling of carbon in a forest on fertile Dark Earth (terra preta do indio) soil in Eastern Amazonia, compared with forest on adjacent infertile soil. *Plant Ecol. Divers.* **7,** 41–53 (2013).
40. Huasco, W. H. *et al.* Seasonal production, allocation and cycling of carbon in two mid-elevation tropical montane forest plots in the Peruvian Andes. *Plant Ecol. Divers.* **7,** 125–142 (2013).
41. Malhi, Y. *et al.* The productivity, metabolism and carbon cycle of two lowland tropical forest plots in SW Amazonia, Peru. *Plant Ecol. Divers.* **7,** 85–105 (2013).
42. Rocha, W., Metcalfe, D., Doughty, C. E. & Mahli, Y. Ecosystem productivity and carbon cycling in intact and annually burnt forest at the dry southern limit of the Amazon rainforest (Mato Grosso, Brazil). *Plant Ecol.Divers.* **7,** 25–40 (2013).
43. Girardin, C. A. *et al.* Productivity and carbon allocation in a tropical montane cloud forest in the Peruvian Andes. *Plant. Ecol. Divers.* **7,** 107–123 (2013).
44. Beck, C., Grieser, J. & Rudolf, B. A new monthly precipitation climatology for the global land areas for the period 1951 to 2000. *Geophys. Res. Abstr.* **7,** 07154 (2005).
45. Fan, Y. & van den Dool, H. A global monthly land surface air temperature analysis for 1948–present. *J. Geophys. Res.* 113**,** D01103, http://dx.doi.org/10.1029/2007jd008470 (2008).
46. Friedl, M. A. *et al.* MODIS Collection 5 global land cover: algorithm refinements and characterization of new datasets. *Remote Sens. Environ.* **114,** 168–182 (2010).
47. Center for International Earth Science Information Network (CIESIN). *Gridded Population of the World, Version 3 (GPWv3): Population Count Grid* http://sedac.ciesin.columbia.edu/gpw (Socioeconomic Data and Applications Center, CIESIN, Columbia University, 2011).

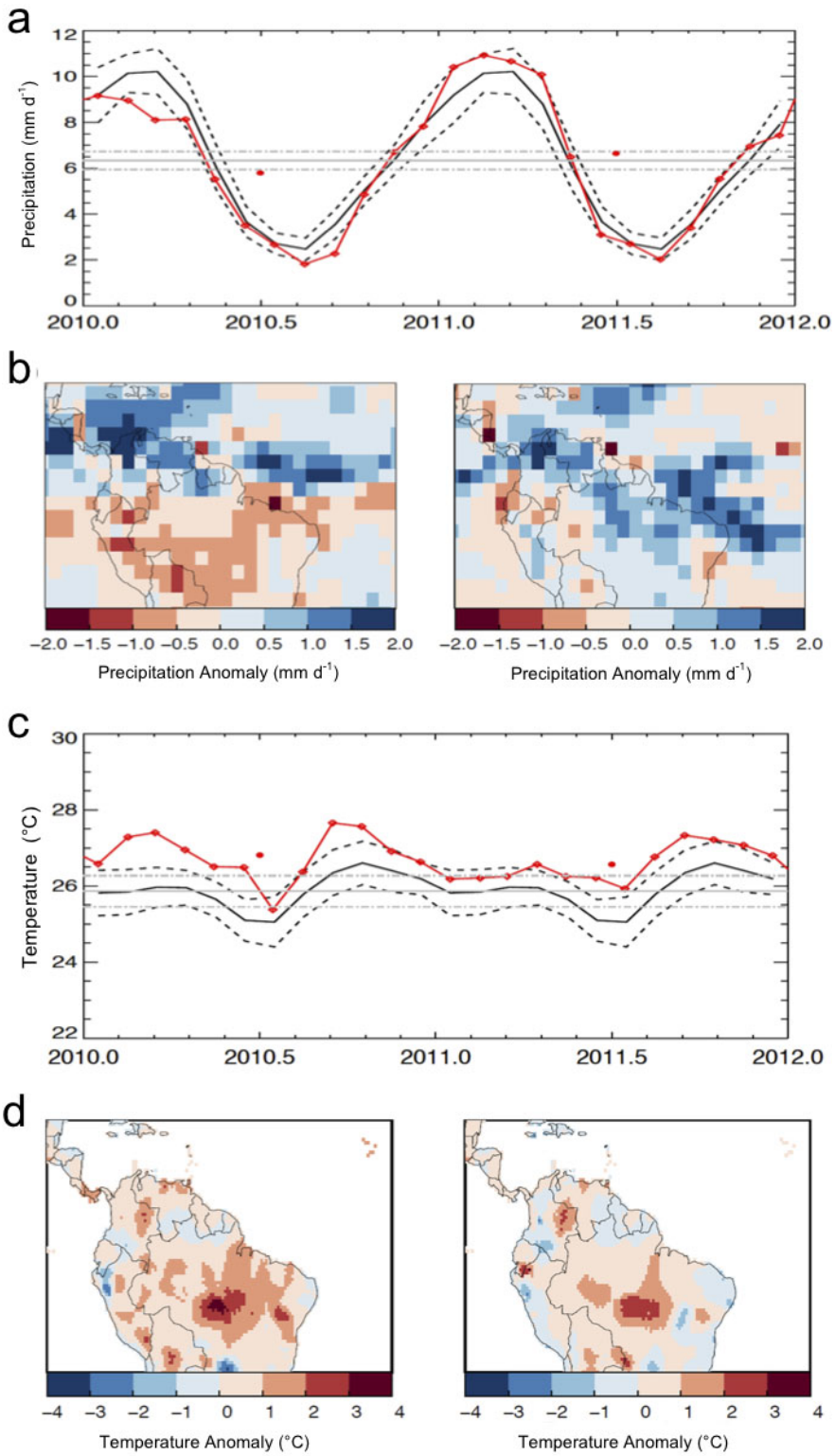

Extended Data Figure 1 | Amazon climate anomalies in 2010 and 2011. **a**, Monthly Southern Hemisphere Amazon basin precipitation from the Global Precipitation Climatology Project (2.5° × 2.5°) for the Southern Hemisphere Amazon basin (accessed from www.esrl.noaa.gov/psd/)[44]. The red line with diamond data points shows the monthly mean precipitation; the black solid line is the 1981–2010 mean and its standard deviation (dashed black lines) for each month. The grey solid line is the annual mean and its standard deviation (dashed grey lines) for 1981–2010 and the filled red circles are annual averages for 2010 and 2011. **b**, Precipitation anomalies in 2010 (left) and 2011 (right) calculated as the annual mean differences from the 1981–2010 averages. **c**, Monthly Southern Hemisphere Amazon basin temperature from the Global Historical Climatology Network version 2 and the Climate Anomaly Monitoring System (0.5° × 0.5°) for the Southern Hemisphere Amazon basin (accessed from www.esrl.noaa.gov/psd/)[45]. The red line with diamond data points shows the monthly mean temperature; the black solid line is the 1981–2010 mean and its standard deviation (dashed black lines) for each month. The grey solid line is the annual mean and its standard deviation (dashed grey lines) for 1981–2010 and the filled red circles are annual averages for 2010 and 2011. **d**, Temperature anomalies in 2010 (left) and 2011 (right) calculated as the annual mean differences from the 1981–2010 averages.

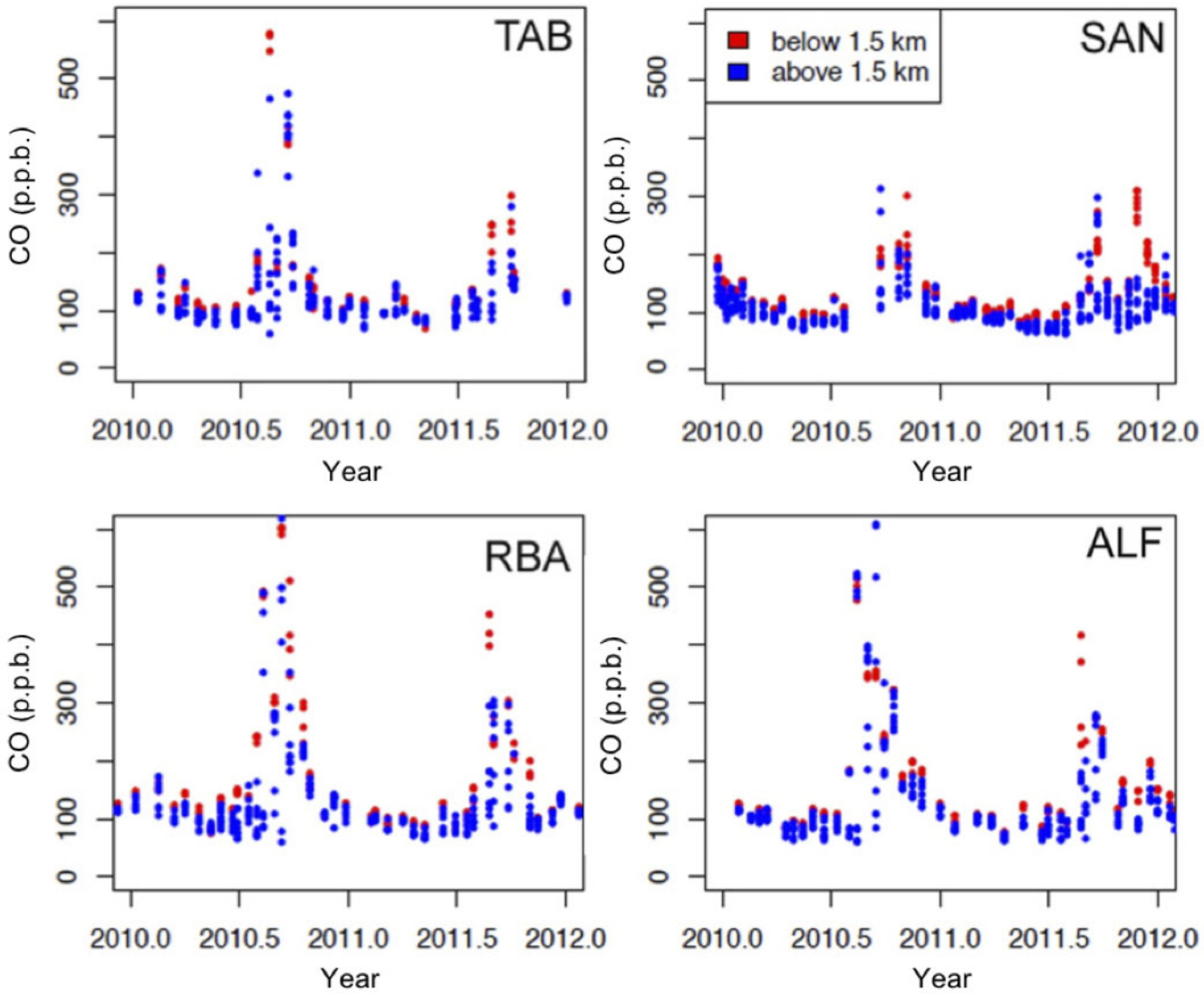

Extended Data Figure 2 | CO concentrations in 2010 and 2011. Data are grouped into above and below 1.5 km height above ground measurements for four sites. p.p.b., parts per billion.

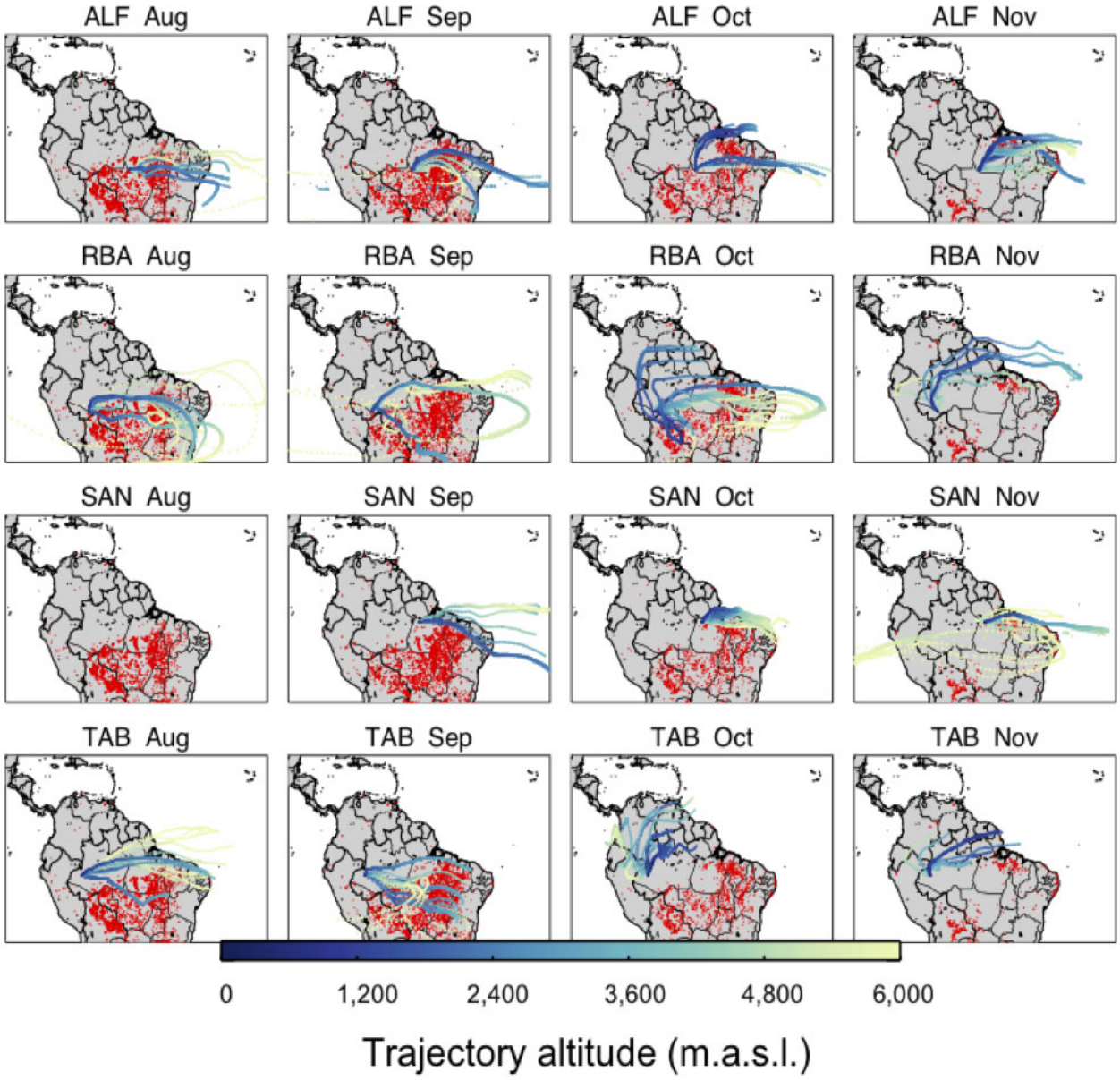

Extended Data Figure 3 | Air parcel paths to measurement sites. Mean seven-day back-trajectories from measurement sites (from FLEXPART) during the 2010 dry season months and fire hotspots from ATSR-WFA, from the Data User Element of the European Space Agency[29].

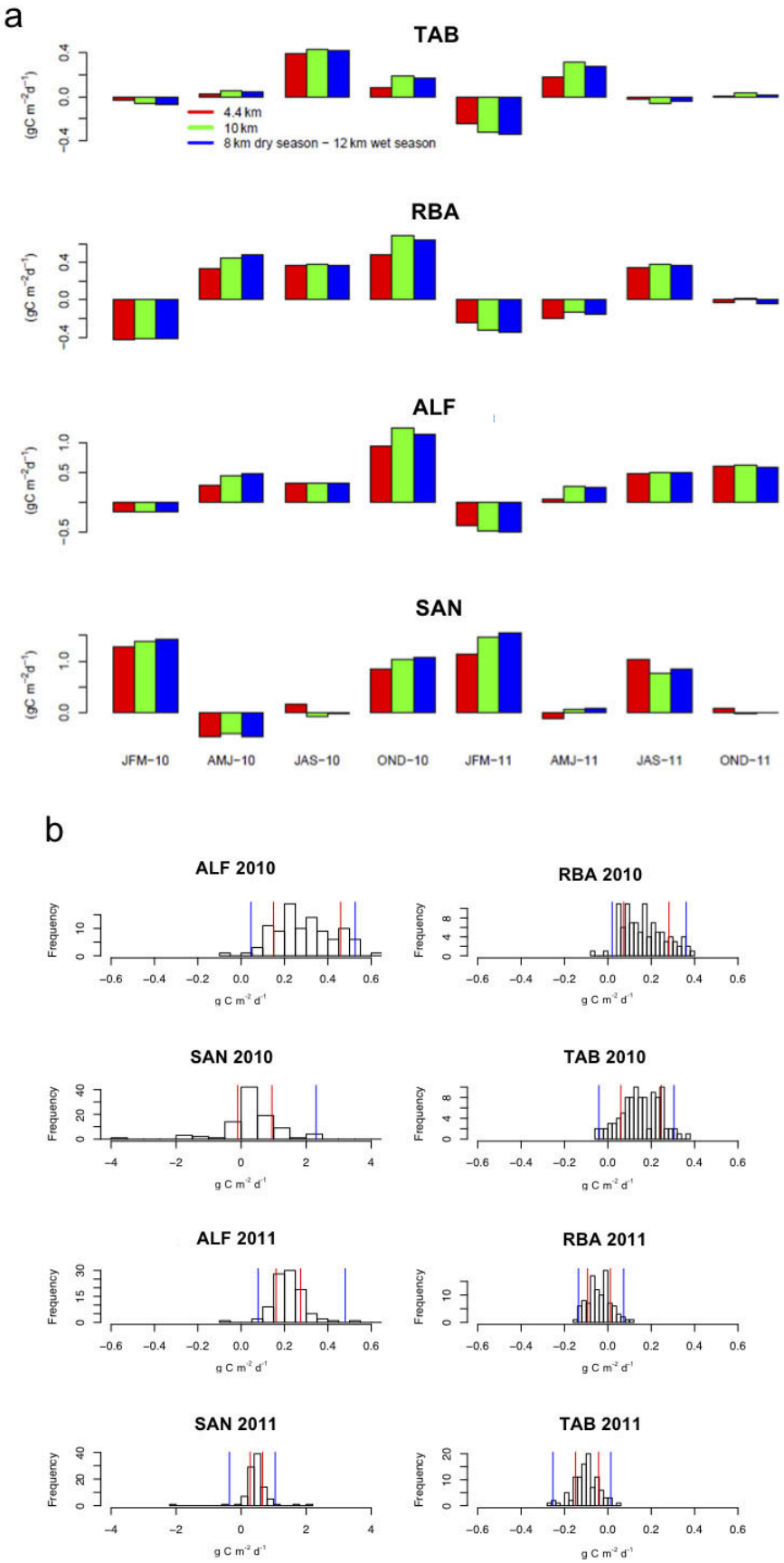

Extended Data Figure 4 | Flux uncertainty statistics. **a**, Sensitivity of flux estimates to profile extrapolation height (months and years are abbreviated below). Comparison of quarterly flux estimates calculated by mass balance of air column up to the top level of measurements (4.4 km a.s.l.), up to 10 km and 8 km a.s.l. during the dry and 12 km during the wet season. **b**, Distributions of annual net carbon flux estimates obtained with Monte Carlo uncertainty propagation (described above) and 68 and 95 percentile intervals of the mean.

a

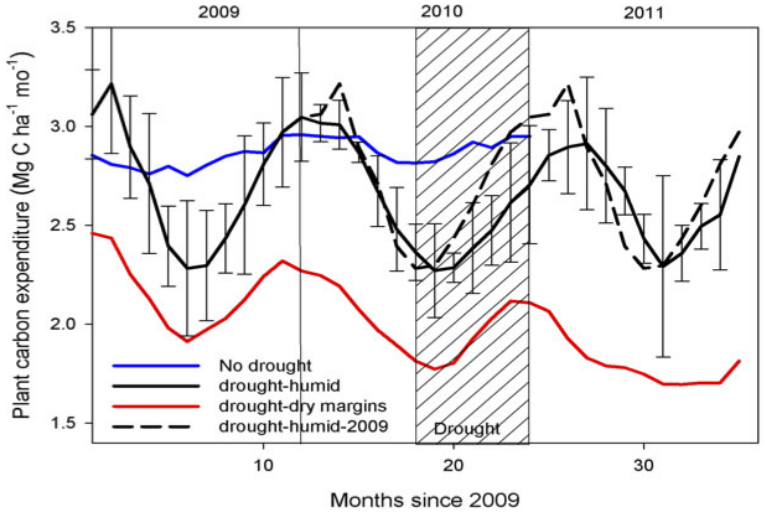

b

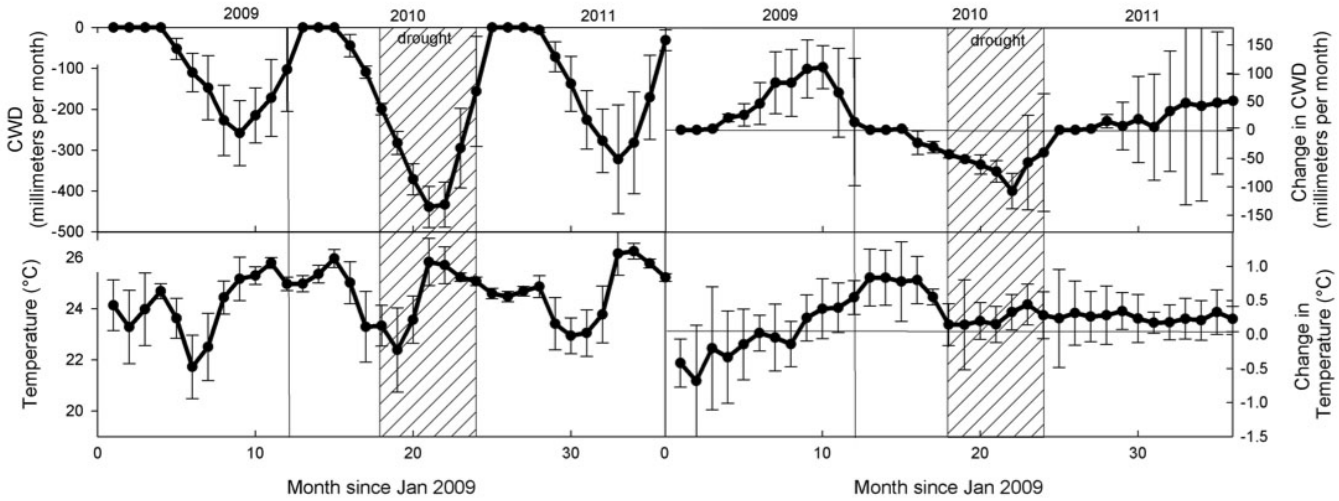

c

Site	Latitude	Longitude
Droughted plots		
Kenia A	16.016 S	62.730 W
Kenia B	16.009 S	62.743 W
Tambopata 3	12.830 S	69,300 W
Tambopata 4	12.834 S	69.297 W
Tanguro	13.077 S	52.390 W
Non-droughted plots		
Caxiuana A	1.737 S	51.462 W
Caxiuana B	1.736 S	51.462 W
Caxiuana Torre	1.720 S	51.458 W
Caxiuana Terra Preta	1.856 S	51.435 W
Kosnipata ESP	13.190 S	71.597 W
Kosnipata SPI	13.047 S	71.543 W
Kosnipata SPII	13.049 S	71.540 W
Kosnipata WAY	13.190 S	71.587 W

Extended Data Figure 5 | Comprehensive forest plot measurement results. **a**, Plant carbon expenditure (NPP plus autotrophic respiration, an upper bound on gross primary production) for 14 1-hectare plots where all NPP and autotrophic respiration components are measured. Eight 1-hectare plots did not experience drought (blue line), six experienced drought, three in the dry lowlands (red line), and three in humid lowland regions ±standard error (black line). The black dashed line is the average seasonal value for 2009 (a typical year) repeated through 2010 and 2011. The hatched bar is the mean drought period for the six drought sites, based on CWD. **b**, Meteorology data from drought plots. Data from Skye instruments meteorology stations from January 2009 to December 2011 near the drought plots (black) for (top left) cumulative water deficit (millimetres per month) and (bottom left) air temperature (in °C). On the right, both plots are the anomalies for the same variable directly to its left with negative values representing a lower than average temperature or precipitation. The hatched bar highlights the approximate period of the 2010 drought in the region based on CWD anomaly. **c**, Intensive carbon balance forest census sites.

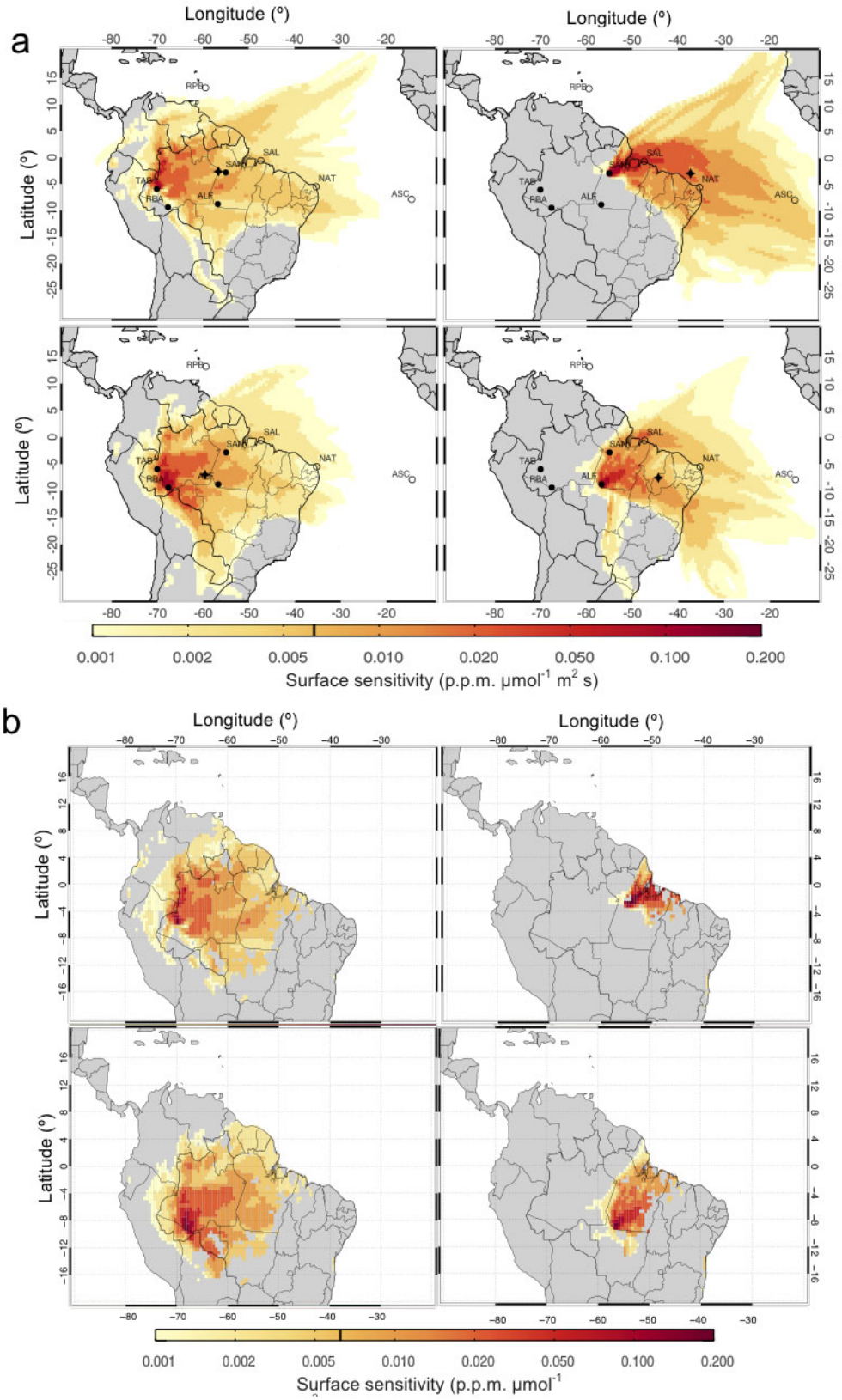

Extended Data Figure 6 | Sensitivity of site atmospheric CO_2 concentrations to surface fluxes. **a**, Sensitivities calculated separately for the four sites (clockwise from the lower left) TAB, RBA, SAN and ALF, and for 2010 calculated with back-trajectory ensembles from the FLEXPART Lagrangian particle dispersion model. The star symbol represents the centroid of the footprint: that is, the point at which footprint contributions are equal to the north and south, and east and west. Note that there is significant overlap of footprints for the 2010 annual mean. **b**, As for **a**, but displaying only the tropical forest biome fraction.

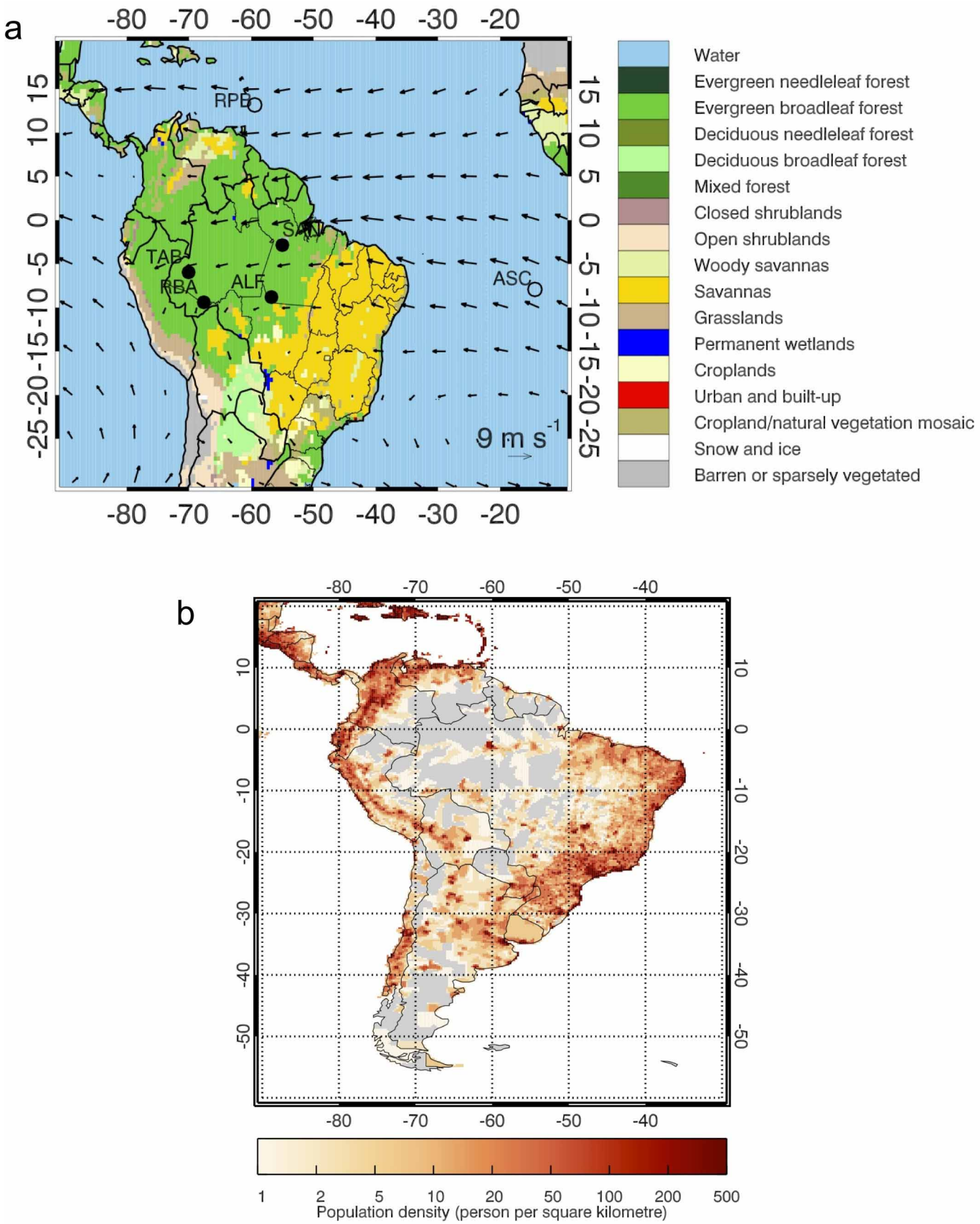

Extended Data Figure 7 | Geographical Summary for South America. **a**, Land cover map of South America from remote sensing (MODIS, Moderate Resolution Imaging Spectroradiometer) obtained from http://modis-land.gsfc.nasa.gov/landcover.html (ref. 46). Black arrows represent average climatological wind speed and direction in June, July and August (from NCEP) averaged between the surface and 600 mbar. **b**, Population density in South America in the year 2005 (ref. 47).

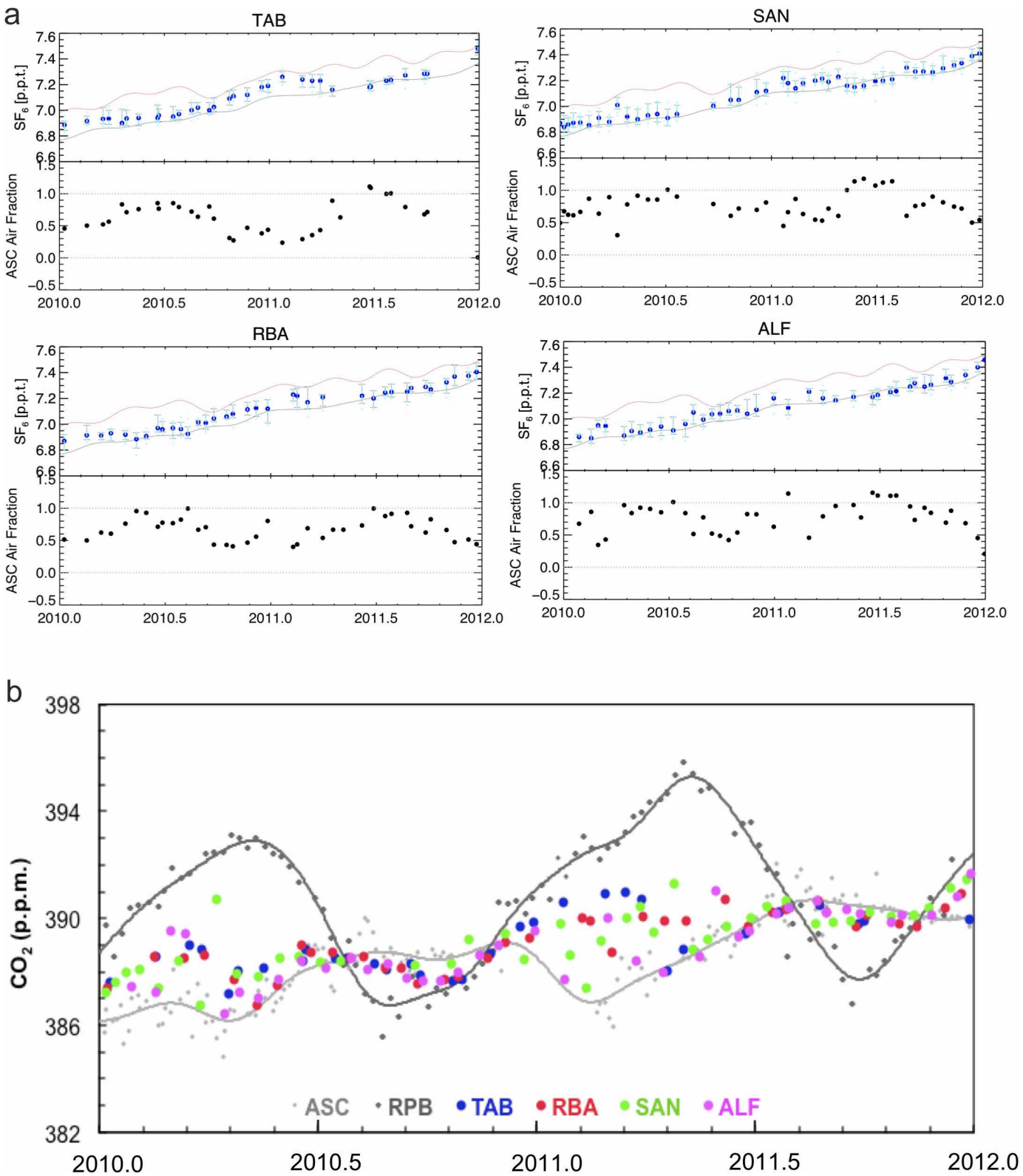

Extended Data Figure 8 | SF_6 and Amazon background concentration calculation. **a**, SF_6 at RPB and ASC and the 'ASC fraction' (f_{ASC}). Data shown for all Amazonian sites. **b**, CO_2 at RPB and ASC and background values estimated based on in situ SF_6 concentrations. Small diamonds (RPB and ASC) represent flask pair averages and thin lines are smooth curve fits to the data[33]. Filled circles (SAN, ALF, TAB and RBA) represent scalar background values for each Amazonian site determined from the smooth curve fits to ASC and RPB and SF_6 values according to equations (4) and (5).

Extended Data Table 1 | Annual flux estimate sensitivity results

a

	2010 flux (g C m^{-2} d^{-1})					2011 flux (g C m^{-2} d^{-1})				
Integration height	4.4 km	8 km	10 km	12 km	Seasonal	4.4 km	8 km	10 km	12 km	Seasonal
TAB										
Total	0.15	0.17	0.18	0.19	0.17	-0.08	-0.09	-0.09	-0.09	-0.09
Fire	0.13	0.15	0.16	0.17	0.16	0.07	0.09	0.10	0.11	0.11
NBE	0.02	0.02	0.02	0.02	0.01	-0.15	-0.18	-0.19	-0.20	-0.20
RBA										
Total	0.18	0.23	0.25	0.27	0.25	-0.02	0.00	0.00	0.00	-0.02
Fire	0.16	0.18	0.19	0.20	0.19	0.08	0.09	0.10	0.10	0.09
NBE	0.02	0.05	0.06	0.07	0.06	-0.10	-0.09	-0.10	-0.10	-0.11
SAN										
Total	0.37	0.37	0.38	0.38	0.40	0.52	0.53	0.53	0.54	0.58
Fire	0.67	0.71	0.73	0.74	0.73	0.50	0.52	0.53	0.53	0.53
NBE	-0.30	-0.34	-0.35	-0.36	-0.33	0.02	0.01	0.00	0.01	0.05
ALF										
Total	0.26	0.33	0.36	0.39	0.35	0.24	0.27	0.28	0.30	0.27
Fire	0.27	0.30	0.31	0.32	0.30	0.13	0.14	0.15	0.15	0.14
NBE	-0.01	0.03	0.05	0.07	0.05	0.11	0.12	0.13	0.15	0.13

[#] Profile integration to 8 km during dry season, and 12 km during wet season.

b

	TAB	RBA	SAN	ALF
	Total Flux (g C m^{-2} d^{-1})			
HYSPLIT	0.15	0.18	0.37	0.26
FLEXPART	0.18	0.19	0.60	0.25
BRAMS	0.22	0.27	0.67	0.30
	Fire Flux (g C m^{-2} d^{-1})			
HYSPLIT	0.13	0.18	0.67	0.27
FLEXPART	0.13	0.17	0.61	0.27
BRAMS	0.13	0.19	0.62	0.32

[#] Using integration height of 4.4 km a.s.l.

a, Sensitivity to integration height. b, Sensitivity of 2010 fluxes to back trajectory travel time.

Extended Data Table 2 | Basinwide annual total fluxes

	4.4 km	10 km	Seasonal	Anti-seasonal
	2010 (Pg C yr^{-1} #)			
Total	0.48	0.61	0.62	0.65
Fire	0.51	0.59	0.59	0.61
NBE	-0.03	0.02	0.03	0.04
	2011 (Pg C yr^{-1} #)			
Total	0.06	0.14	0.12	0.16
Fire	0.29	0.34	0.33	0.35
NBE	-0.23	-0.20	-0.21	-0.19

assuming 6.77 x 10^6 km^2 total basin area[30]